Available online at www.sciencedirect.com

jmr&t Journal of Materials Research and Technology

journal homepage: www.elsevier.com/locate/jmrt

Original Article

Tensile behavior of crack-repaired ultra-high-performance fiber-reinforced concrete under corrosive environment

Doo-Yeol Yoo [a,*], Taekgeun Oh [a], Wonsik Shin [a,b], Soonho Kim [a], Nemkumar Banthia [c]

[a] Department of Architectural Engineering, Hanyang University, 222 Wangsimni-ro, Seongdong-gu, Seoul, 04763, Republic of Korea

[b] R&D Center, Samwoo IMC, 269 Jungdae-ro, Songpa-gu, Seoul, 05660, Republic of Korea

[c] Department of Civil Engineering, The University of British Columbia, 6250 Applied Science Lane, Vancouver, BC, V6T 1Z4, Canada

ARTICLE INFO

Article history:
Received 16 June 2021
Accepted 23 November 2021
Available online 26 November 2021

Keywords:
Ultra-high-performance fiber-reinforced concrete
Crack repair
Steel fiber corrosion
Tensile performance
Crack width

ABSTRACT

This study aims to evaluate the influence of crack repair using epoxy sealing on the tensile response of ultra-high-performance fiber-reinforced concrete (UHPFRC) under corrosive environments. Three different crack widths, i.e., 0.1, 0.3, and 0.5 mm, and two different corrosion durations, i.e., 4 and 10 weeks, were considered. The test results indicated a minor change in the tensile performance of UHPFRC with the smallest crack width of 0.1 mm under corrosive environments for up to 10 weeks. This is due to the restriction of ferric oxide formation at the densified fiber–matrix interface. A wider crack width accelerated the steel fiber corrosion and noticeably influenced the post-cracking tensile behavior. Considering the corrosion duration of 4 weeks, the tensile strength of cracked UHPFRC with a width of 0.3 mm or greater increased by approximately 12–17% owing to the moderate steel fiber corrosion. However, the tensile strength decreased during the longer corrosion duration of 10 weeks by ruptures of excessively corroded steel fibers. Crack repair using epoxy sealing increased the tensile strength of cracked UHPFRC by approximately 10% and effectively prevented further corrosion of steel fibers at the crack location, leading to higher tensile strength even after 10 weeks of corrosion.

1. Introduction

Various fiber-reinforced concrete (FRC) types have been developed over the decades using high-modulus materials, such as steel and carbon, or ductile, low-modulus materials, such as polyvinyl alcohol (PVA), polypropylene (PP), and nylon [1–6]. When compared to other synthetic fibers, steel fibers have been considered as an appropriate structural reinforcement for various applications, such as reinforced concrete

* Corresponding author.
E-mail address: dyyoo@hanyang.ac.kr (D.-Y. Yoo).

https://doi.org/10.1016/j.jmrt.2021.11.121

(RC) beams with low reinforcement ratios and concrete tunnel linings, owing to the high elastic modulus, stiffness, and interfacial adhesion to a brittle cement matrix [7–9]. As a representative ductile, low-modulus fiber—PP fiber—is known to be effective in preventing plastic shrinkage cracks in concrete because of its good ductility, fineness, and dispersion [10,11] in terms of durability. In early 2000, Naaman and Reinhardt [12] classified FRCs under tension and flexure based on the softening or hardening characteristics regardless of the fiber type. They [12] suggested that hardening materials are useful in structural applications, while deflection-softening materials cover a wide range of applications, such as the control of plastic shrinkage cracks, pavements, and slabs on grade.

As an advanced technology, ultra-high-performance fiber-reinforced concrete (UHPFRC) was introduced in the mid-1990s in France [13], and it has been considered to be appropriate for structural applications (e.g., irregular buildings, long-span bridges, and slender (foot)bridges [14–16]) because of its strain-hardening characteristics and the use of steel fibers [17,18]. Its densified microstructures, formed by a low water-to-binder ratio and incorporation of high-fineness ingredients, can achieve excellent compressive strength that is greater than 150 MPa [19] and durability [20]. Voort [20] reported that the resistance to chloride-ion penetration of UHPFRC is 220 and 34 times higher than those of normal and high-performance concretes, respectively. Hence, pristine UHPFRC exhibits excellent resistance to steel fiber corrosion [21–23] and overcomes the shortcomings of ordinary steel fiber-reinforced concrete (SFRC) [24]. Although SFRC has better resistance to the ingress of chloride ions (Cl^-) and is more durable than conventional RC [25], its deterioration in strength and toughness has also been observed by steel fiber corrosion under corrosive environments [24]. In contrast, Hashimoto et al. [21] reported marginal steel fiber corrosion and chloride-ion penetration up to 6 months in UHPFRC, and the corrosion process of steel fibers in ultra-high-performance concrete (UHPC) was very slow, causing the corrosion of the exposed steel fibers only [23].

Owing to the susceptibility of UHPFRC to early age shrinkage cracks at the manufacturing stage caused by the rapid development of autogenous shrinkage and small cross-sectional areas, tiny microcracks are however frequently formed in UHPFRC elements [26], which can be potential pathways for Cl^- ingress. Berrocal et al. [27] reported drastic decrease of corrosion initiation period of steel in concrete as it is cracked. Recently, the deteriorated corrosion resistance of steel fibers in cracked UHPFRC has been found [21,28]. Deep Cl^- penetration in cracked UHPFRC with a width of 0.5 mm or greater was detected [21], and severely corroded steel fibers ruptured prematurely, which deteriorated the tensile performance of UHPFRC [28]. French standard (NF P 18–710) [29] recommended the maximum allowable crack width of 0.3 mm or below for UHPFRC under various environmental conditions. The structural integrity is not reduced by the (micro-) cracks formed during the manufacturing stage or service state, but it should be repaired in terms of aesthetics and long-term durability. Very few studies [21,23,28,30] are only available on steel fiber corrosion in UHPC, and there are no published studies on the steel fiber corrosion in crack-repaired UHPFRC yet.

This study investigated the effect of crack repair based on epoxy sealing on the steel fiber corrosion in UHPFRC. The repaired and non-repaired UHPFRC specimens were immersed in a 3.5% standard NaCl solution for up to 10 weeks with pre-crack widths of 0.1–0.5 mm. The corrosion degree of the steel fibers at the exposed and embedded portions near the crack plane was evaluated using a confocal laser scanning microscope, and its influence on the tensile response of UHPFRC was analyzed using direct tensile tests. Crack repair effectively inhibited the steel fibers from further corrosion and suppressed the decrease in the tensile strength at the longest corrosion duration of 10 weeks by preventing the premature ruptures of steel fibers before the pullout.

2. Experimental program

2.1. Materials and mixing sequence

To evaluate the tensile behavior of crack-repaired UHPFRC using epoxy sealing under corrosive environments, the UHPC matrix surrounding the steel fibers was first mixed. Several types of dry ingredients, such as Type I ordinary Portland cement (OPC), silica fume (SF), silica flour as a filler, and silica sand as a fine aggregate, were prepared. The chemical compositions of the cement materials (OPC and SF) are given in Table 1. The main chemical compositions of OPC and SF are calcium oxide (CaO) and silicon dioxide (SiO_2), respectively. Although silica flour is mainly composed of SiO_2, it is considered as an inert filler owing to its coarser particle sizes [31]. The particle size distributions of all dry ingredients are shown in Fig. 1. The order of mean grain size is as follows: silica sand (337 μm) > OPC (22 μm) > silica flour (4.2 μm) > SF (0.31 μm). To achieve a very high compressive strength of the UHPC matrix, a water-to-binder (W/B) ratio was adopted to be 0.2 (Table 2). A high-range water-reducing agent (superplasticizer) was also added to obtain sufficient workability with self-consolidating properties. A high-volume fraction (2 vol.%) of long straight steel fibers, having a diameter of 0.3 mm and length of 30 mm, was incorporated into the UHPC mixture to fabricate UHPFRC, because based on previous studies performed by Yoo et al. [32,33], the use of straight steel fiber with an aspect ratio of 100 was more effective on improving the tensile (or flexural) performance of UHPC as compared to that with a lower aspect ratio of around 65, frequently used for commercial products. The density and tensile strength of the

Table 1 – Chemical compositions of OPC and SF.

Composition %	OPC	SF
SiO_2	18.8	92.60
Al_2O_3	4.18	0.07
Fe_2O_3	3.72	0.49
CaO	65.3	0.67
MgO	2.43	1.80
SO_3	3.28	0.12
Na_2O	0.15	0.02
K_2O	1.1	–

[Note] OPC = ordinary Portland cement and SF = silica fume.

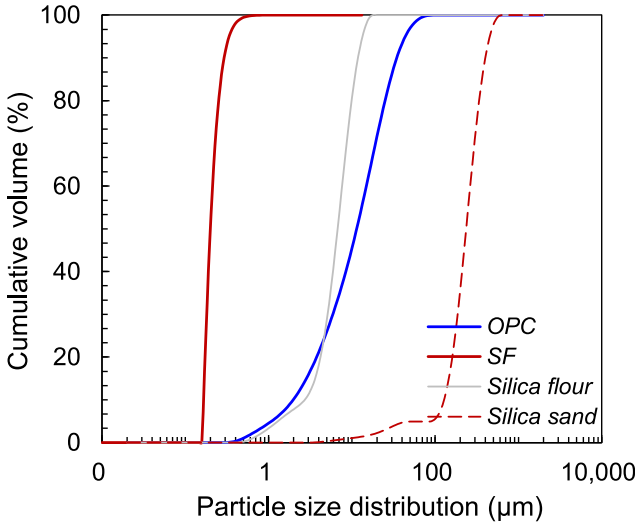

Fig. 1 – Particle size distribution of dry ingredients.

used steel fibers were approximately 7.9 g/cm^3 and 2580 MPa, respectively. The detailed mix proportions of the UHPC and UHPFRC are listed in Table 2.

All dry ingredients were first added to a Hobart-type mixer and premixed for 10 min. Water mixed with the superplasticizer was then added and mixed 10 min more. A flowable fresh UHPC was formed that was used to prepare fiber pullout test samples. To fabricate the UHPFRC, 2 vol.% steel fibers were carefully added and mixed for 5 min. The fresh UHPFRC was used to prepare direct tensile dog-bone samples. The compressive strength was found to be about 210 MPa, as per ASTM C39 [34], and it had very low porosity of around 6%, similar to other types of UHPC [35] and much lower than that of ordinary cement paste [36].

2.2. *Single fiber pullout test*

Because UHPFRC is known to exhibit strain-hardening behavior, the post-cracking tensile properties are highly influenced by the fiber bridging curve. The bridging effect of straight steel fibers from the cement matrix is related to the interfacial friction, which can be evaluated from a fiber pullout test. Hence, a dog-bone-shaped sample with a cross-sectional area of 25 × 25 mm^2, consistent with that used in a previous study by Farooq and Banthia [37], was fabricated and tested. The geometrical details of dog-bone specimen are given in Fig. 2a. A single straight steel fiber was initially fixed at the center of the mold using a very thin PVC film with an embedded length of 10 mm. Then, the fresh UHPC matrix was cast on one side of the mold with an embedment length of 10 mm and 48-h cured in a laboratory room. Subsequently, the other side of the mold was filled with the fresh UHPC and cured for the same time in the laboratory room. Park et al. [38] recommended an initial curing at 20 °C for 24 h and steam curing at 90 °C for 48 h to achieve a specific compressive strength of 180 MPa. Thus, to promote strength development and achieve the specific strength, the dog-bone samples were demolded and stored in a water tank at a high temperature of approximately 90 °C for 72 h.

To evaluate the pullout resistance of steel fibers from epoxy-based repair materials, dog-bone samples were fabricated based on the repair material. After fixing the single steel fiber at the center of the mold, one side was filled with the repair material and cured in the laboratory room for 48 h, and the other side was filled with the same material and cured in the same room for another 48 h. Then, they were demolded and stored in a room at a constant temperature (23 °C) and relative humidity (50%) (as recommended by the product data sheet) for 14 days before testing. The dog-bone samples fabricated using UHPC and the repair material are shown in Fig. 2c.

Fig. 2b shows the details of test setup. The dog-bone sample was inserted in a steel grip system with a roller to allow rotation. Then, a uniaxial pullout load was applied through a universal testing machine (UTM) at a rate of 0.018 mm/s. The applied load was measured from the affixed load cell to the machine, and the stroke displacement was adopted as the fiber slip by assuming negligible elastic deformations of the sample and jig. Several previous studies [39,40] also directly measured the fiber slip from vertical displacement by assuming the neglected elastic deformation of the fiber and specimen. To obtain reliable average data, eight dog-bone samples were used for each variable.

2.3. *Direct tensile test*

Fig. 3a shows the geometrical details of the dog-bone sample made of UHPFRC for the direct tensile test in accordance with JSCE recommendations [41]. Its cross-sectional area was 13 × 30 mm^2 with 7.5-mm notches on both sides. Owing to its small cross-sectional size, better fiber alignment to the direction of flow was expected to be obtained as compared to in-situ concrete. The notches were made using a diamond blade to induce a single crack with widths of 0.1, 0.3, and 0.5 mm. The total length of each sample was 330 mm. The mold was

Table 2 – Mix proportion of UHPC.

	W/B[b]	Mix design [kg/m^3]						v_f [%]
		Water	Cement	Silica fume	Silica sand	Silica flour	SP[a]	
UHPC	0.2	160.3	788.5	197.1	867.4	236.6	52.6	–
UHPFRC								2.0

[Note] UHPC = ultra-high-performance concrete, UHPFRC = ultra-high-performance fiber-reinforced concrete, W/B = water-to-binder ratio, SP = superplasticizer, and v_f = fiber volume fraction.

[a] SP includes 30% solid (= 15.8 kg/m^3) and 70% water (=36.8 kg/m^3).

[b] W/B is calculated by dividing total water contents (160.3 kg/m^3 + 36.8 kg/m^3) by total amount of binder (788.5 kg/m^3 + 197.1 kg/m^3).

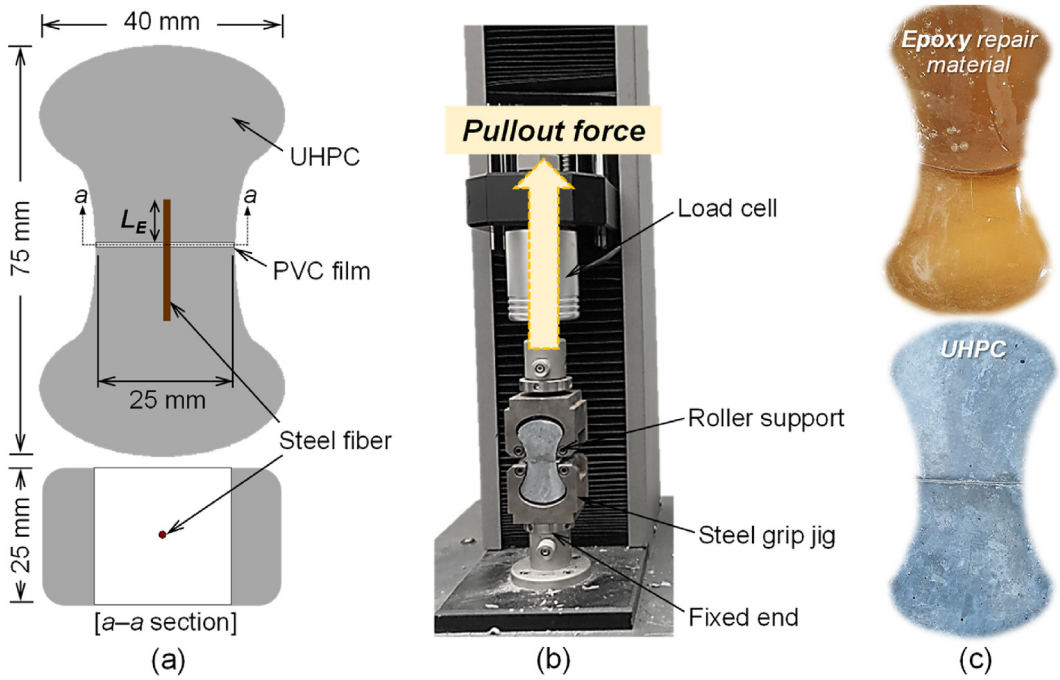

Fig. 2 – Single fiber pullout test setup: (a) geometrical detail, (b) picture of test setup, and (c) dog-bone samples made of UHPC and epoxy repairing material.

prepared, and fresh UHPFRC was cast parallel to the longitudinal direction of the sample to obtain better fiber alignment and consistent tensile properties [42]. Then, the exposed surface was immediately covered with a plastic sheet for the prevention of abrupt water evaporation.

The direct tensile test setup is shown in Fig. 3b. The dog-bone sample was inserted in the steel grip jig, and uniaxial tensile force was uniformly applied by the UTM. A pin and fixed support condition was adopted in order to minimize the eccentric effect. A clip gauge with a capacity of 5 mm was installed at the tip of the notches to measure the crack mouth opening displacement (CMOD). The applied load was recorded from a load cell attached to the testing machine. To investigate the crack width effect on the steel fiber corrosion, the dog-bone samples were loaded and unloaded to obtain residual CMODs of approximately 0.1, 0.3, and 0.5 mm. Certain CMOD values were first determined based on trial and error to provide the residual CMOD values of 0.1, 0.3 and 0.5 mm. Then, it was applied equally for all tested samples. The maximum differences to the target residual CMODs were 0.035, 0.044 mm, and 0.052 mm for the cases of 0.1, 0.3 and 0.5 mm, respectively.

2.4. *Corrosion process*

Van Belleghem et al. [43] reported that, for cracked concrete, an active state of corrosion is detected within an exposure period of 10 weeks. The pre-cracked UHPFRC samples were thus submerged in a standard 3.5% NaCl solution for 28 and 70 days (4 and 10 weeks). In accordance with a previous study by Roventi et al. [44], wet–dry cycles for 7 days each were adopted to accelerate the corrosion process of steel fibers. After 28 and 70 days of this process, the pre-cracked samples were dried in the laboratory until the testing date. To evaluate the effect of crack repair on the inhibition of steel fiber corrosion, half of the 4-week corroded UHPFRC samples were repaired by epoxy-based material and then re-corroded for another 6 weeks to obtain an identical corrosion duration of 10 weeks. The detailed corrosion process is illustrated in Fig. 4.

2.5. *Crack repairing process using epoxy sealing*

The purpose of this study is to evaluate the effect of crack sealing on the corrosion resistance of steel fiber in UHPFRC. To repair pre-induced cracks in UHPFRC, an epoxy-based repair material was thus adopted [45]. This material was prepared by mixing two types of components at a ratio of 2:1 using a mixer at a rate of 400–600 rpm for 3 min. Because the repair material was flowable and had low viscosity, the tiny cracks in UHPFRC could be effectively sealed. Selection of proper type of repair material is important because its effectiveness is dependent on the inherent diffusivity in terms of chloride ions and an ability to penetrate and fill the cracked regions [46].

Fig. 4 shows the repair process of the cracked UHPFRC sample using epoxy-based repair material. It was induced by the mixed repair material after enclosing the notched region through the PVC board and hot melt adhesive. Then, the samples were stored in a chamber at a constant temperature (23 °C) and relative humidity (50%) for 14 days to cure the crack repair material, as recommended by the manufacturer [45]. Subsequently, they were reloaded by the UTM after installation of the clip gauge to measure the tensile stress and CMOD curves.

The test variables were divided into three categories: plain (Pl), pre-cracked (Pr), and corroded (C) samples. For the Pr and C samples, the sequential numbers denote the crack widths of

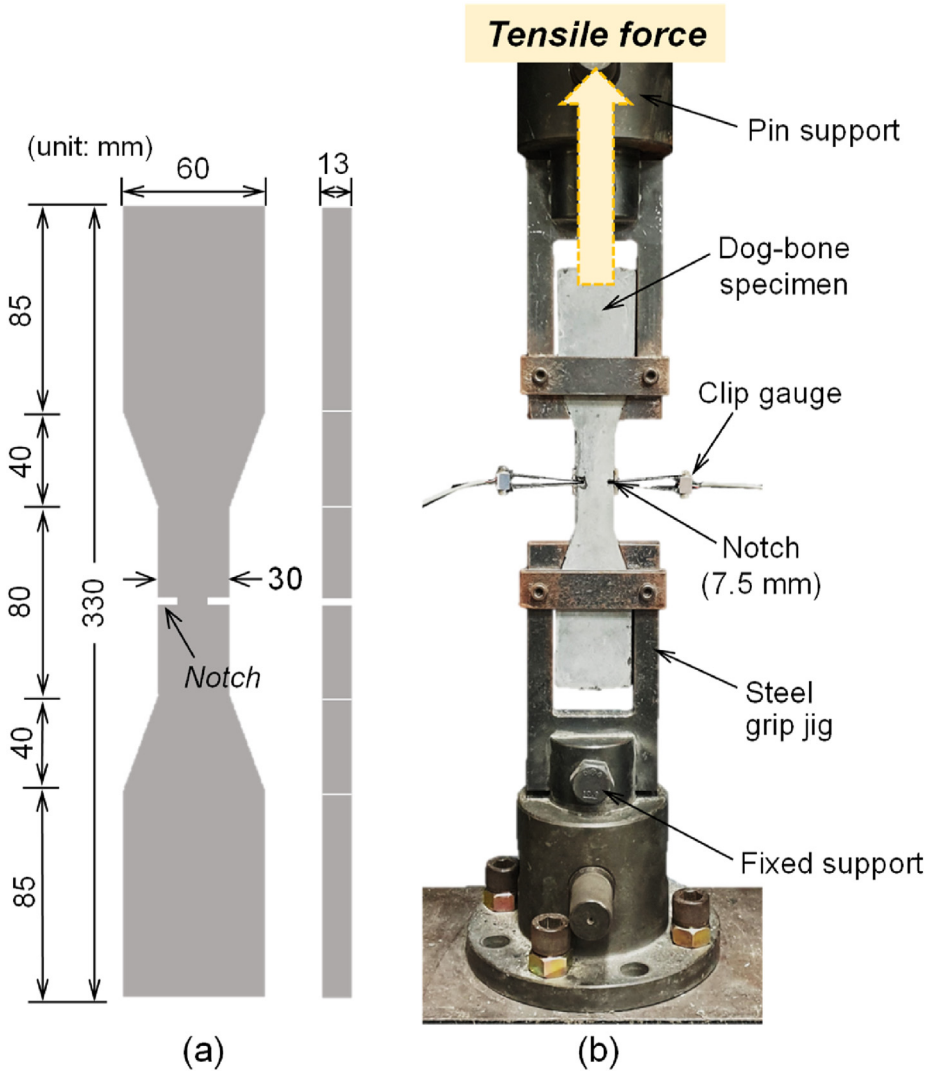

Fig. 3 – Direct tensile test setup of notched UHPFRC sample: (a) geometrical detail and (b) picture of test setup.

0.1, 0.3, and 0.5 mm, and the letters after a hyphen indicate the duration of the corrosion process; for example, 4 weeks, 10 weeks, and 4 weeks + 6 weeks after repair. "R" denotes the repaired sample. For example, C0.1-10 indicates a sample with a crack width of 0.1 mm submerged in the NaCl solution for 10 weeks, while C0.1–4R6 denotes a sample with a crack width of 0.1 mm submerged in the NaCl solution for 4 weeks initially and another 6 weeks more after the repair process.

2.6. *Microscope image analysis*

To quantitatively evaluate the surface state of steel fibers, a confocal laser scanning microscope (LEXT™ OLS5100, Olympus) with high accuracy and optical performance was used. After the completion of tensile tests, the steel fibers were initially extracted from the UHPFRC composites. Each steel fiber was then used for three-dimensional scanning along its longitudinal direction, and 128.75 × 128.75 μm^2 scanning data were attached three times based on a stitching method, leading to 1:3 stitching data. The line roughness on the fiber surface was evaluated at three random locations by specifying a measurement line after data acquisition, and the width of the measurement line was 3 μm for eliminating noise. The microscope images on the surface of steel fibers were taken at three different locations, such as exposed, boundary, and embedded regions, to evaluate the effects of crack width and fiber/matrix interfacial condition on the corrosion degree of steel fibers from the cracked UHPFRC under corrosive environments.

3. Experimental results and discussion

3.1. *Comparative pullout behavior of steel fiber from UHPC and repair material*

An epoxy-based repair material is used to repair cracks in the UHPC samples to prevent progressive steel fiber corrosion by permeation of NaCl solution through cracks. To investigate the corrosion effect of steel fibers on the tensile performance of the repaired UHPFRC, the repair material needs to have a minor effect on the fiber bridging strength. Thus, the pullout

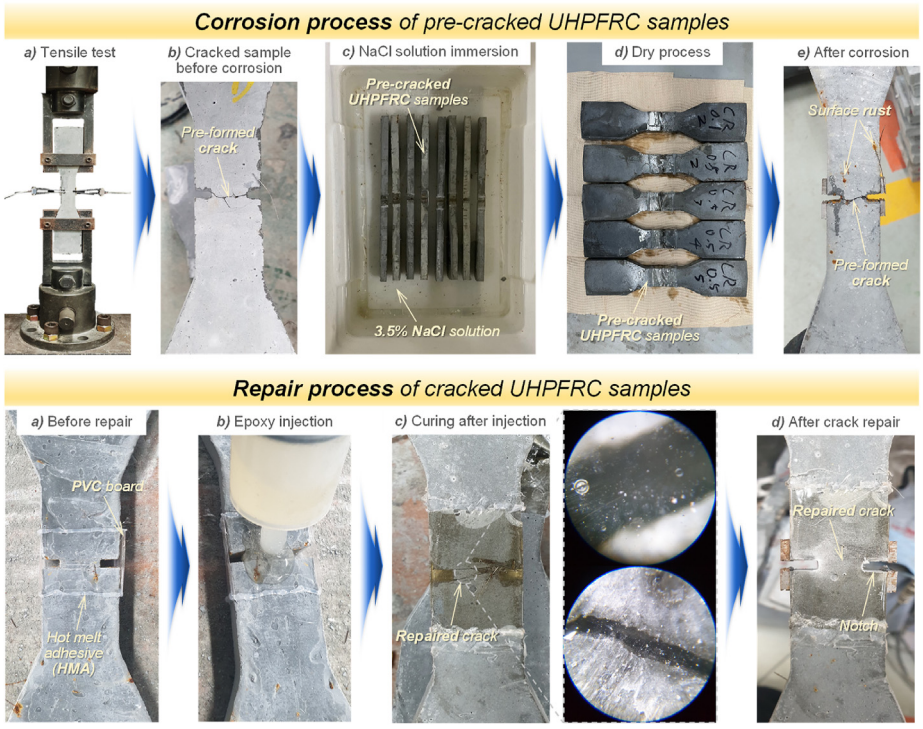

Fig. 4 – Corrosion and repair processes of cracked UHPFRC.

behaviors of single steel fibers embedded in the UHPC and repair material are compared in Fig. 5. Owing to the densified interfacial zone between the fiber and UHPC matrix, a very high average bond strength of 7.73 MPa was observed, similar to the bond strengths, i.e., 7.5–9 MPa, reported by Wille and Naaman [47] for brass-coated straight steel fibers embedded in various UHPC mixes. A gradual decrease in the post-peak pullout load was also detected via the abrasion of the steel fiber surface and slight end deformation in the UHPC in Fig. 5a. Even though identical steel fibers and embedment lengths of 10 mm were adopted, poorer pullout resistance was detected in the repair material. A moderate anchorage effect due to end deformation was not detected. An average bond strength of 1.70 MPa was obtained in the repair material case, which was approximately 22% of that of the UHPC matrix. Its pullout energy (84.6 mJ) was also approximately 18% of the pullout energy of the UHPC (475.5 mJ), shown in Fig. 5b. These observations verify that the main role of epoxy-based repair material is to fill the cracks to prevent permeation of the NaCl solution, and its influence on the tensile performance of cracked UHPFRC will be small.

3.2. *Tensile behavior*

Fig. 6 compares the tensile stress and CMOD curves of control and pre-cracked UHPFRC samples with various crack widths of 0.1, 0.3, and 0.5 mm. By adopting identical volume fraction (2%) of steel fibers and casting method, the tensile behaviors of pre-cracking UHPFRC samples up to a certain width of 0.3 mm or 0.5 mm were very similar to that of the plain sample

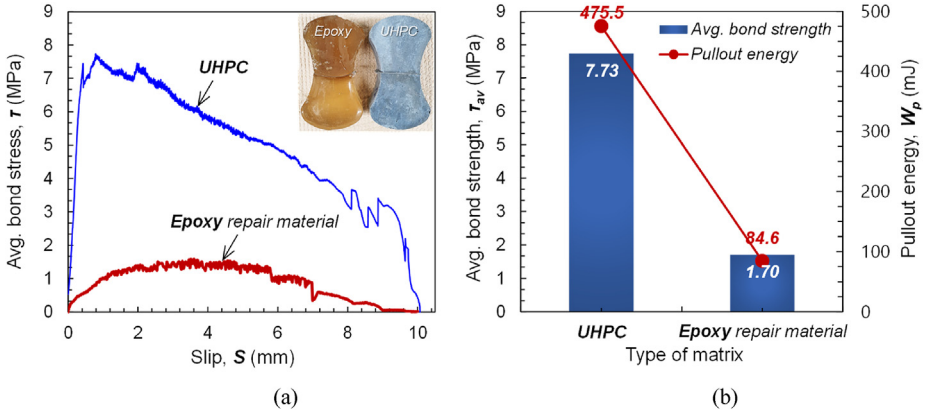

Fig. 5 – Pullout behaviors of straight steel fibers from UHPC and epoxy-repairing matrices: (a) average bond stress–slip curves and (b) pullout parameters.

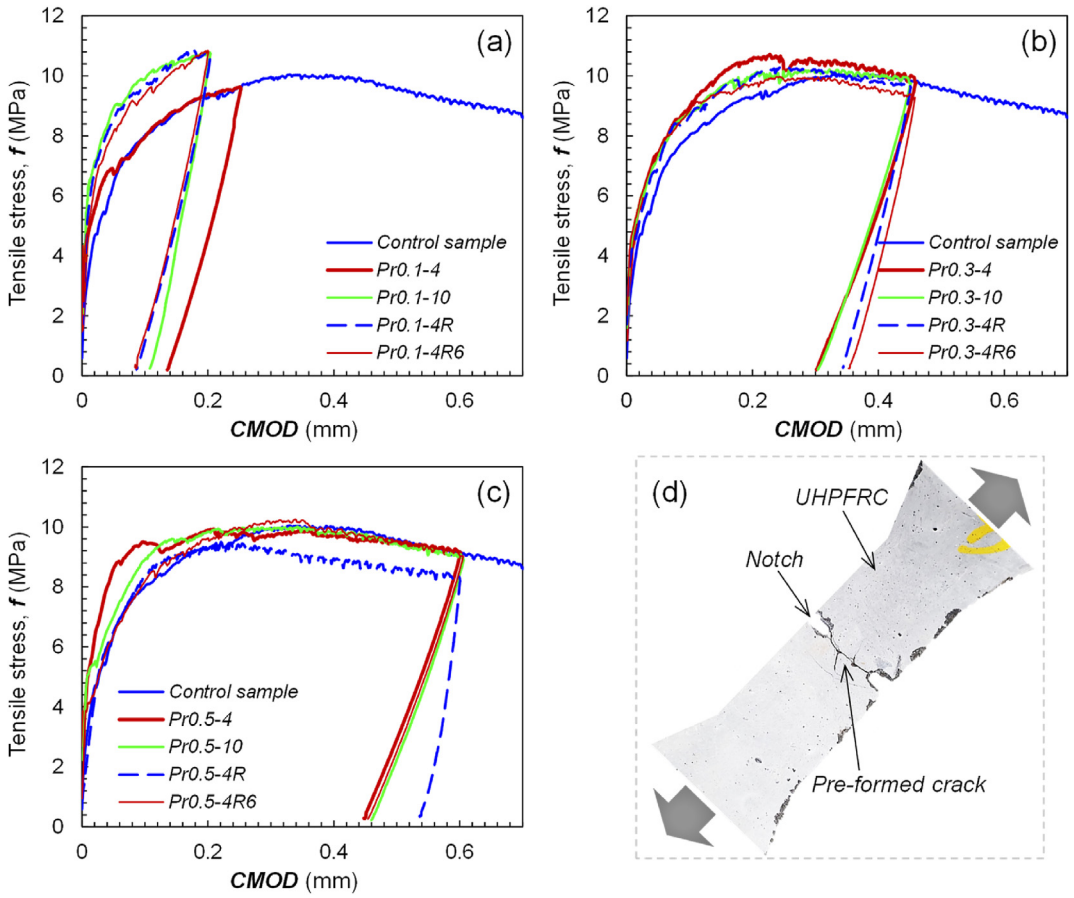

Fig. 6 – Comparative tensile stress and CMOD curves of control and pre-cracking samples with crack widths of (a) 0.1 mm, (b) 0.3 mm, and (c) 0.5 mm and (d) picture of typical pre-cracked sample.

(Fig. 6b and c) that enables a reasonable analysis of the steel fiber corrosion effect. However, the 0.1-mm pre-cracked samples provided higher post-cracking stiffness and tensile stress at the unloading portion as compared to the control sample in general, except for the Pr0.1-4 sample (Fig. 6a). This might be because although the dog-bone samples were carefully fabricated by the same casting method, the pre-cracking samples contained more steel fibers near the center notch due to the random orientation and inhomogeneous dispersion of steel fibers. The higher post-cracking stiffness and level of tensile stress at the unloading point are thus considered when the steel fiber corrosion effect on the tensile behavior is analyzed subsequently.

3.2.1. *Influences of crack width and corrosion duration on the tensile response of UHPFRC*

Fig. 7 summarizes the average tensile stress–CMOD curves of plain, pre-cracked, and corroded UHPFRC samples. In the case of 4-week corrosion, the tensile strength of the pre-cracked UHPFRC with crack widths of 0.3 mm or higher increased after immersion in the NaCl solution due to the moderately corroded steel fibers. Yoo et al. [48] reported an increased interfacial bond strength between the steel fiber and UHPC matrix owing to its surface corrosion up to a certain corrosion degree of 2%. The reason for the enhanced interfacial friction is the increased surface roughness because of the formation of corrosion products [49]. Ngo et al. [50] also observed the increased pullout resistance of deformed steel fibers in high-performance concrete as they were corroded up to a certain corrosion level. With a crack width of 0.3 mm or higher, the pre-cracked UHPFRC samples were included in the post-peak softening region, indicating that a portion of the steel fibers at the crack plane began to slip from the UHPC matrix. Ferric oxide (Fe_2O_3) can be formed on the surface of steel fibers in UHPC when it is chemically debonded [51]. Thus, the steel fibers in the C0.3- and C0.5-4 samples could be easily corroded through the fully debonded interfacial zone, leading to an increase in tensile strength. To evaluate the increase rate of tensile strength by steel fiber corrosion, the tensile strength of the corroded sample (σ_{cr}) was divided by the tensile stress of the pre-cracked samples at the point of unloading (σ_{pr}), as shown in Fig. 7. Considering the pre-crack width of 0.1 mm, the maximum tensile stress was used as the value of σ_{pr} as it is located in the ascending region, while the tensile stresses at the CMODs of 0.45 and 0.6 mm were determined as the values of σ_{pr}, which are the unloading portions for the Pr0.3 and Pr0.5 series based on several preliminary tests. If there is no effect of steel fiber corrosion on the tensile behavior, the ratio σ_{cr}/σ_{pr} must be equal to 1 for the case of 0.3- or 0.5-mm crack width. However, ratios of 1.169 and 1.118 were observed in the samples with crack widths of 0.3 and 0.5 mm, respectively, indicating that the tensile strengths increased by

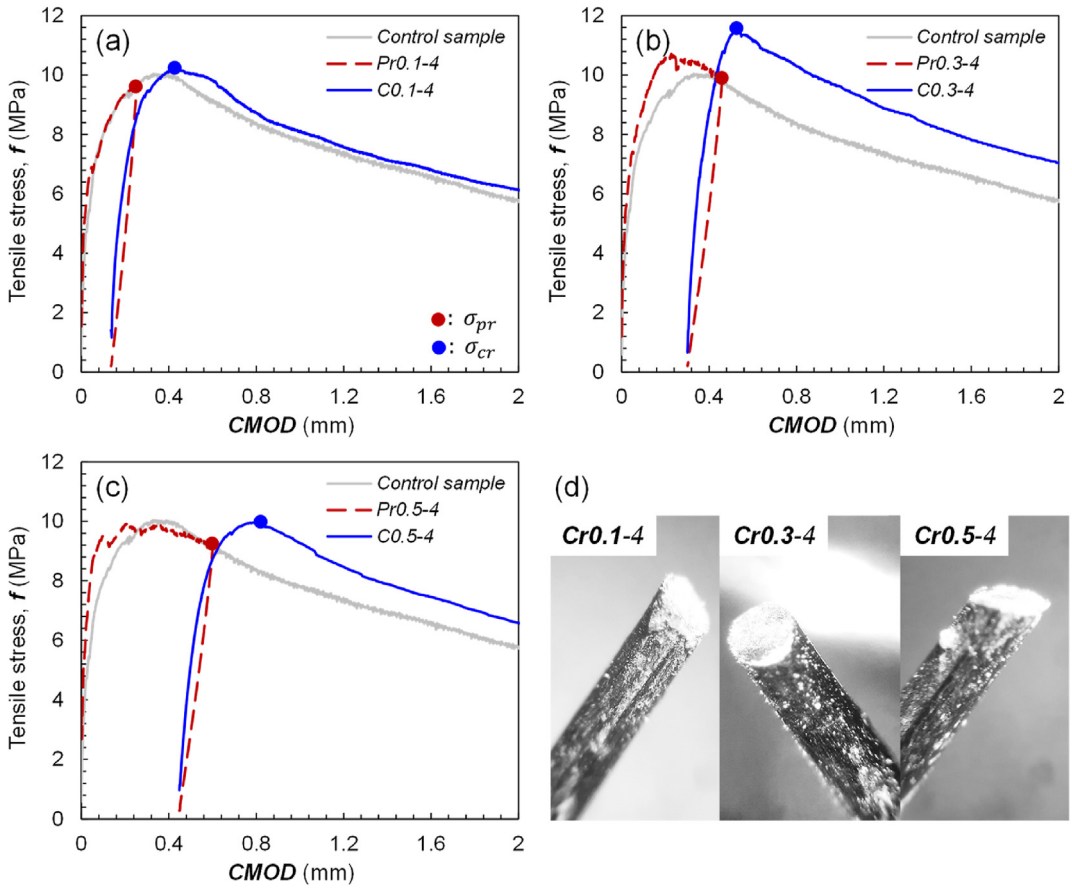

Fig. 7 – Comparative tensile stress and CMOD curves of control, pre-cracking, and 4-week corroded samples with crack widths of (a) 0.1 mm, (b) 0.3 mm, and (c) 0.5 mm and (d) typical picture of pulled out steel fibers.

approximately 11.8–16.9% owing to steel fiber corrosion. It can be considered that there is no apparent increase in the tensile strength detected in the C0.1-4 sample (Fig. 7a) because of the insufficient interfacial gap between the fiber and matrix to create Fe_2O_3. Although the tiny crack was not completely filled with self-healing material, e.g., $CaCO_3$, it might be partially filled with the $CaCO_3$ that helps to suppress the steel fibers from corrosion. The tensile strength of the C0.1-4 sample appeared to be located at the end of the ascending region of the stress–CMOD curve of control sample. This means that a wider crack width accelerates the corrosion of steel fibers in the UHPC matrix and strongly influences its post-cracking tensile performance. Further, owing to the shorter immersion duration of 4 weeks that lead to a moderate corrosion degree, all steel fibers at the crack plane were pulled out completely from the matrix without any breakage (Fig. 7d).

In order to support the above explanations, the surface states of steel fibers located at the localized crack planes were analyzed through the microscope images in Fig. 8. At the exposed region, the steel fiber surfaces were corroded with a formation of rust regardless of the pre-crack width. However, the amounts of Fe_2O_3 formed on the surface of steel fiber were influenced by the crack width. Owing to the smaller crack width of 0.1 mm, a small portion of steel fiber surface was covered by the rust, compared to the larger crack width (≥0.3 mm). This indicates that greater crack width leads to more severe corrosion of steel fibers in cracked UHPFRC at the exposed region. To verify the above observations, the height profiles that were averaged at five random locations are compared in Fig. 9. The roughest fiber surface was detected at the exposed region equally, whereas relatively flat and smooth surface was detected at the embedded region. The significantly changed height profiles at the embedded region were caused by the formation of Fe_2O_3, and the wider crack width led to the larger fluctuations of height profiles, indicating more severe corrosion. We also calculated the surface roughness parameter, R_a, based on the following equation [52], to quantitatively evaluate the degree of surface roughness of steel fibers by corrosion.

$$R_a = \frac{1}{n}\sum_{i=1}^{n}|z_i| \quad (1)$$

where n is the number of data used and y_i is the height of the i^{th} point in nm.

In Fig. 10, the surface roughness at the exposed region increased with the crack width from 0.1 mm to 0.5 mm. For example, the highest value of R_a was found in the C0.5-4 sample by 4.28 μm, approximately 426% and 239% times higher than those of C0.1- and C0.3-4 samples, respectively. The microscope image, height profile, and roughness parameter thus all indicated the more severe corrosion of steel fibers with the greater crack width. Since the rust on the surface of

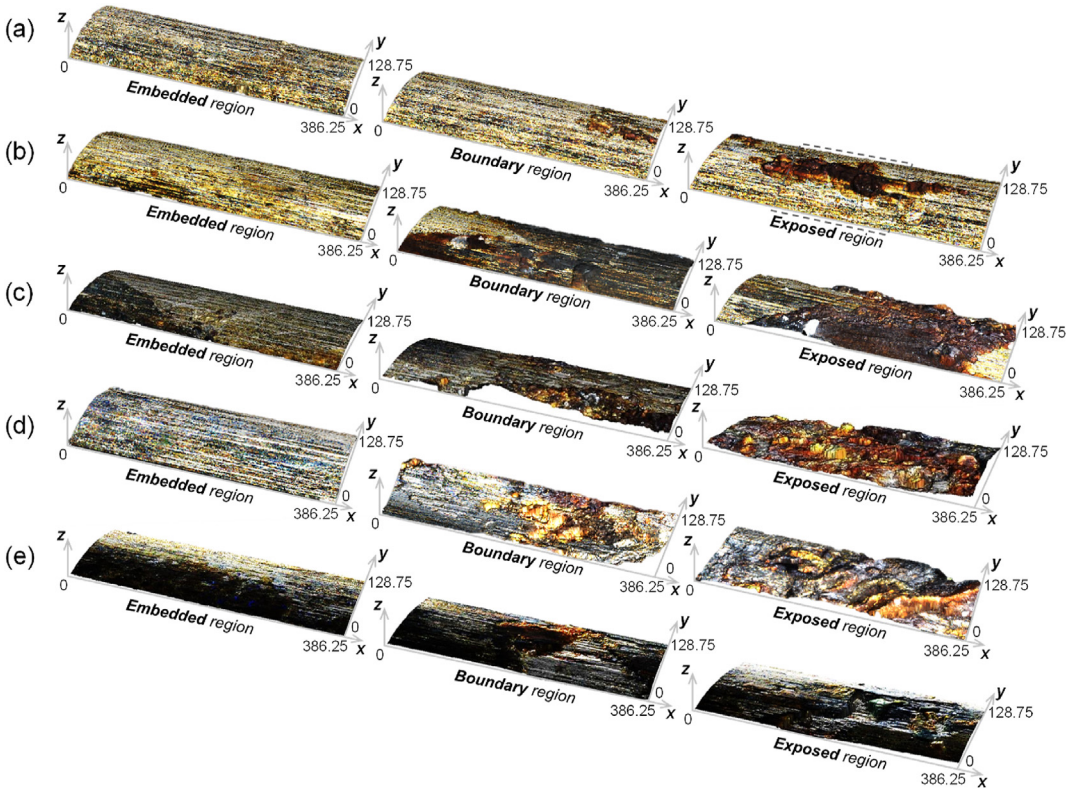

Fig. 8 – Microscope images of pulled out steel fibers at embedded, boundary, and exposed regions: (a) C0.1-4, (b) C0.3-4, (c) C0.5-4, (d) C0.3-10, and (e) C0.3–4R6.

steel fiber could be effectively detected through the microscope images in Fig. 8, the chemical monitoring was not conducted.

The variation of post-cracking tensile performance of UHPFRC in terms of steel fiber corrosion is closely related to the interfacial bond behavior. Therefore, to evaluate the corrosion degree on the steel fiber surface at the embedded region, the microscope images were also taken at two different locations: 1) near the fiber exit (boundary region) and 2) 1–1.5 mm apart from the crack plane (embedded region). As

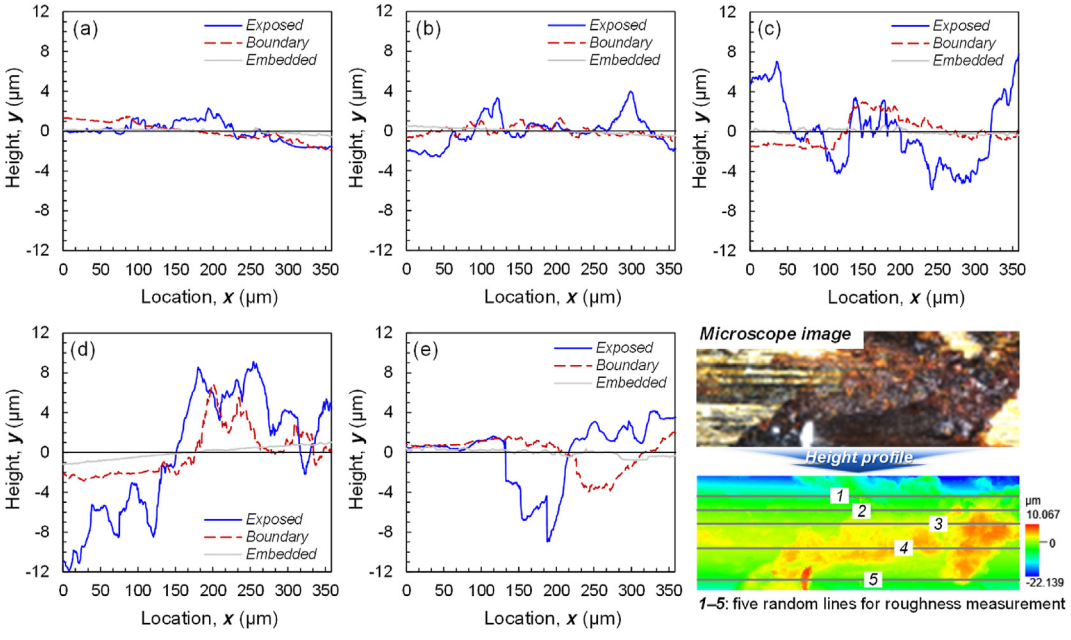

Fig. 9 – Comparison of surface roughness of pulled out steel fibers at embedded, boundary, and exposed regions: (a) C0.1-4, (b) C0.3-4, (c) C0.5-4, (d) C0.3-10, and (e) C0.3–4R6.

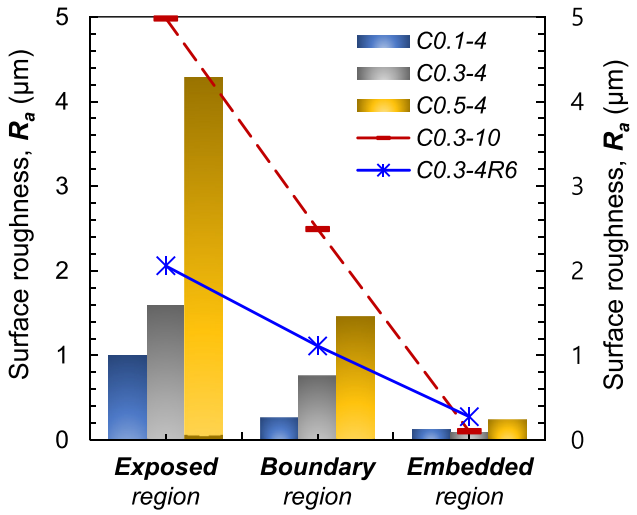

Fig. 10 – Summary of roughness parameter (R_a).

shown in Fig. 8, the surface of steel fibers extracted from the C0.1-4 samples was relatively cleaner than those extracted from the C0.3- and C0.5-4 samples at the boundary region. The steel fiber surface seemed to be more severely corroded with the increased crack width. This could be verified by roughness measured along the fiber length in Figs. 9 and 10. The steel fiber pulled out from the C0.5-4 sample provided the highest roughness parameter, R_a, of 1.46 μm, followed by the C0.3-4 sample (R_a of 0.76 μm) and the C0.1-4 sample (R_a of 0.26 μm). This is caused by a formation of more rust. Some ferric oxides detected on the surface of C0.1-4 samples were potentially located at the exposed region, and the rest was embedded in the UHPC matrix and pulled out by the external force. This verifies that the formation of ferric oxide on the embedded surface of steel fiber was difficult and thus the tensile behavior of the C0.1-4 sample was similar to that of the control sample. On the contrary, the vestige of ferric oxide formed at the boundary region was detected in the case of C0.3- and C0.5-4 samples. The ferric oxide formed at the fiber/matrix interface increased the surface roughness and provided confining pressure by expansion, which led to their increased tensile strengths as compared to the control sample. The embedded steel fibers exhibited smooth surface without any rust, regardless of the crack width, meaning that the rust is locally formed at the interface near the fiber exit when it is fully debonded and partially slipped. The locally formed rust thus significantly affected the post-cracking tensile behavior of UHPFRC. Chun et al. [53] reported the continuously increased shear stress at the fiber/matrix interface with the slip, caused by very densified microstructures and slight end deformation. The progressive formation of Fe_2O_3 into the embedded region was thus limited even after the steel fiber was fully debonded from the cement matrix.

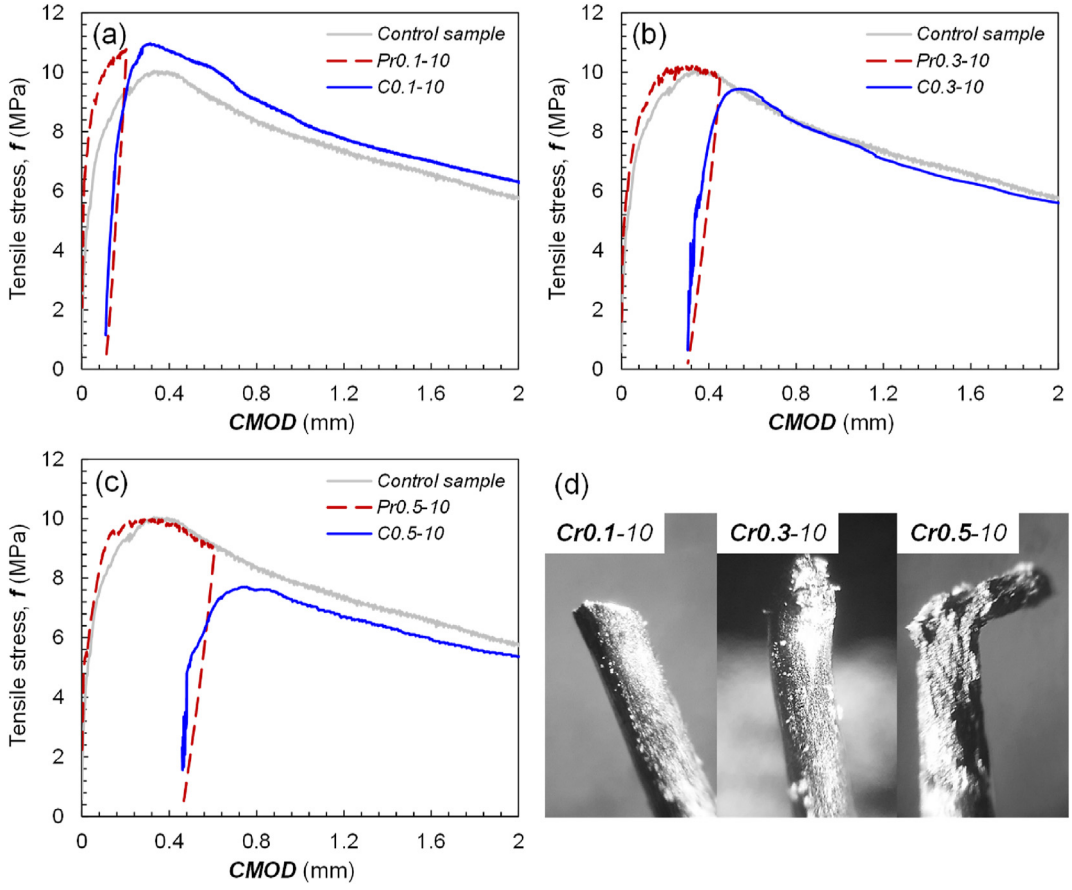

Fig. 11 – Comparative tensile stress and CMOD curves of control, pre-cracking, and 10-week corroded samples with crack widths of (a) 0.1 mm, (b) 0.3 mm, and (c) 0.5 mm and (d) typical picture of pulled out steel fibers.

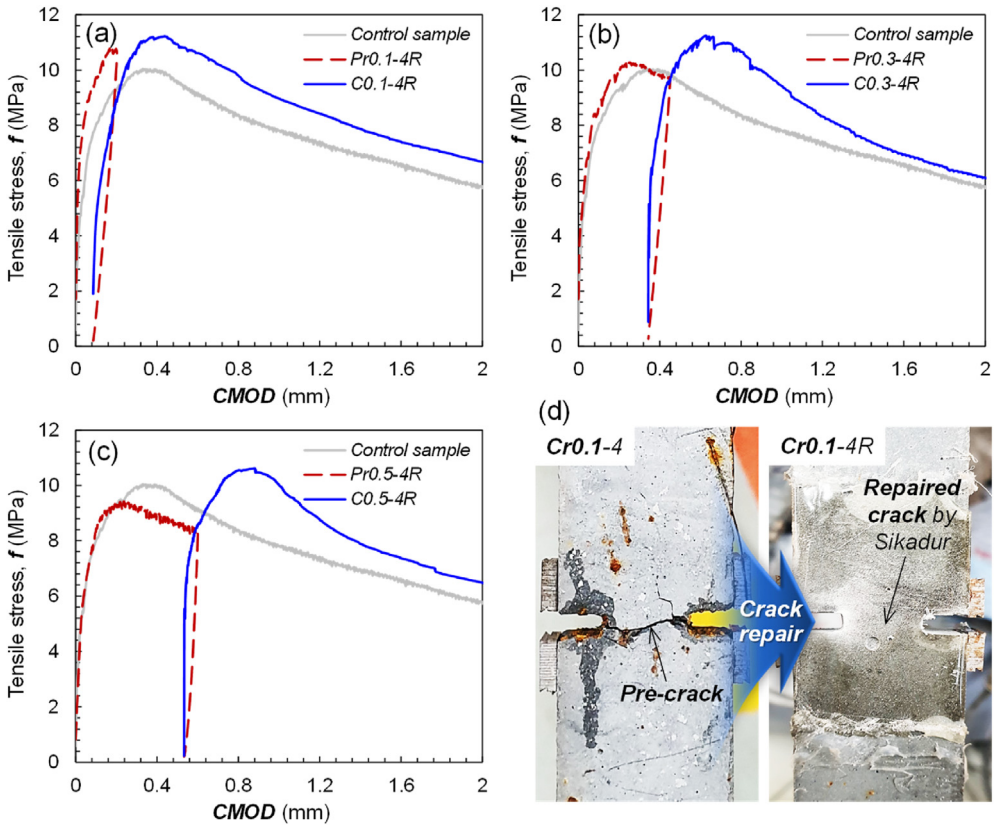

Fig. 12 – Comparative tensile stress and CMOD curves of control, pre-cracking, and 4-week corroded and repaired samples with crack widths of (a) 0.1 mm, (b) 0.3 mm, and (c) 0.5 mm and (d) picture of before and after crack repair.

The comparative tensile behaviors at the longer immersion duration of 10 weeks are shown in Fig. 11. For the case of the smallest crack width (0.1 mm), the tensile behavior of UHPFRC did not change according to the corrosion process (Fig. 11a), which is similar to the shorter duration of 4 weeks. In contrast, the increased tensile strengths of C0.3- and C0.5-4 samples, due to the moderate steel fiber corrosion, were mitigated at a longer duration of 10 weeks, as shown in Fig. 11b and c. In the case of the C0.5-10 sample, the tensile strength reduced as compared to that of the Pr0.5-10 sample without corrosion. Longer exposure to corrosive environments (3.5% NaCl solution in this study) is known to aggravate the corrosion degree of steel fibers caused by the continuous release of Fe^{2+} and formation of ferric oxide, which could be verified by the microscope images in Fig. 8. The steel fiber surface of C0.3-10 samples was more covered by ferric oxides at both the exposed and boundary regions. In addition, the values of R_a for the C0.3-10 were much higher than those for the C0.3-4 at the exposed and boundary regions in Fig. 10. This is consistent with the findings of Frazão et al. [54] who reported greater progress of corrosion phenomenon in steel fibers with the immersion time. The enhanced interfacial friction and decreased cross-sectional area of the steel fibers led to premature breakage in the UHPC matrix that limited the further increase in the tensile strength. As illustrated in Fig. 8, the surface of steel fiber at the embedded region of the C0.3-10 sample was not corroded, like the C0.3-4 sample. Thus, they provided similar surface roughness (Fig. 10). It could be noted that the steel fiber corrosion in UHPC is progressed slowly, and the ferric oxide locally formed at the interface near the fiber exit significantly influenced the tensile behavior of UHPFRC. The surface roughness of C0.3–4R6 was slightly higher than that of C0.3-4, which might be caused by the remained NaCl solution at the crack plane and fiber–matrix interfacial zone. However, the surface roughness of C0.3–4R6 was much lower than that of C0.3-10, given the identical corrosion duration, indicating that the epoxy injection is effective for limiting the further steel fiber corrosion.

To verify the fiber failure mode at the crack plane, magnified images were captured, as shown in Fig. 11d. Most steel fibers in the C0.1-10 sample were completely pulled out from the matrix without any breakage, whereas many ruptured steel fibers were detected in the C0.3- and C0.5-10 samples because of excessive steel fiber corrosion. Their σ_{cr}/σ_{pr} ratios were lower than those of the 4-week samples and found to be 0.999 and 0.886 for the C0.3- and C0.5-10 samples, respectively. This indicates that the tensile strength of the 0.5-mm cracked UHPFRC decreased by approximately 11.4% owing to the severely corroded steel fibers for 10 weeks. Thus, it is concluded that the UHPFRC with a wider crack width is vulnerable to steel fiber corrosion because the steel fibers at the crack plane are fully debonded to the surrounding cement matrix and partially slip, resulting in the easier formation of ferric oxide on their surface. The earlier deterioration of pullout resistance of fully debonded steel fibers from UHPC when compared to that of partially debonded fibers was

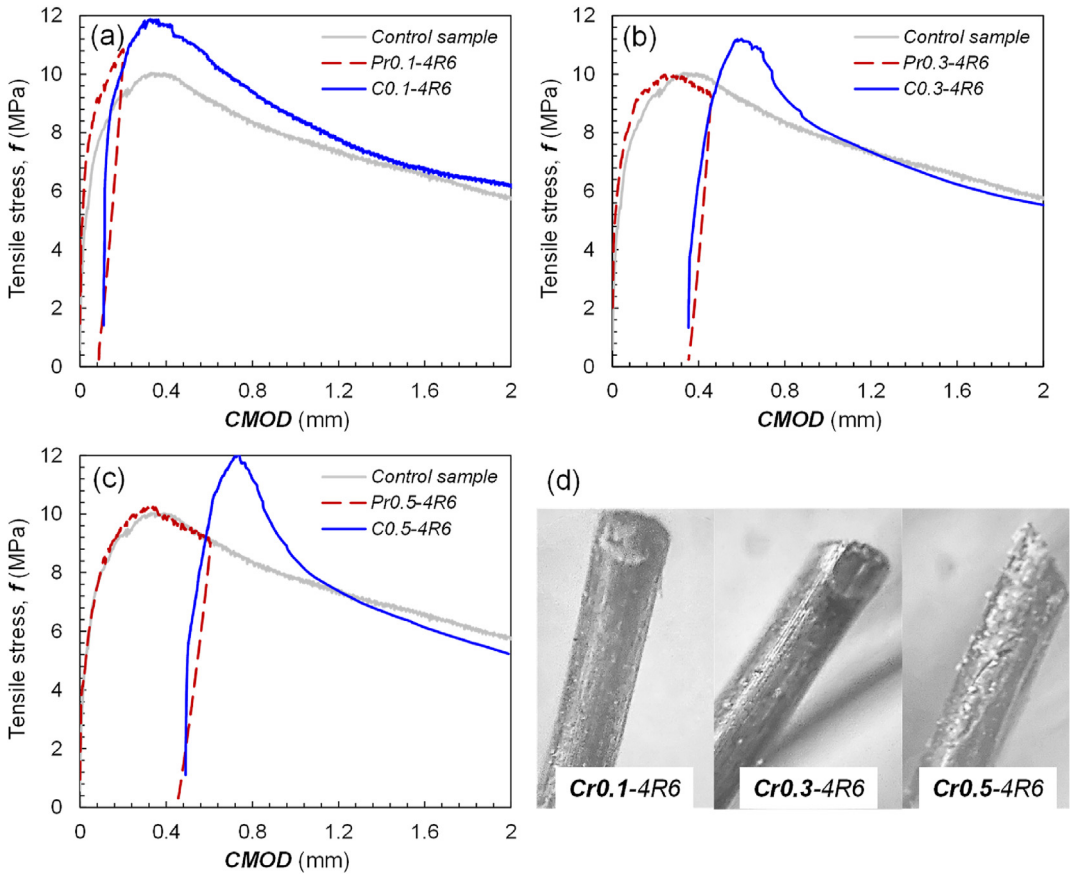

Fig. 13 – Comparative tensile stress and CMOD curves of control, pre-cracking, and 4-week corroded, repaired, and 6-week re-corroded samples with crack widths of (a) 0.1 mm, (b) 0.3 mm, and (c) 0.5 mm and (d) picture of before and after crack repair.

verified by Yoo et al. [51]. Hashimoto et al. [21] noted that non-cracked UHPFRC shows marginal steel fiber corrosion and penetration of chloride ions for up to 6 months, while apparent steel fiber corrosion and deep penetration of chloride ions were detected in the cracked UHPFRC with a crack width ≥0.5 mm French standard (NF P 18–710) [29] also suggested maximum allowable crack width of 0.3 mm for UHPFRC under dry or permanently wet condition. Given severer conditions (e.g., cyclic wet and dry), the smaller allowable crack width of 0.2 mm was recommended for reinforced and unbonded prestressed UHPFRC members. These findings and recommendations [21,29] are consistent with the results of this study.

3.2.2. *Influence of crack repair on the tensile response of UHPFRC under corrosive environment*

To evaluate the influence of crack repair on the inhibition of progressive corrosion of steel fibers at the crack plane, we conducted direct tensile tests on the 4-week corroded samples after crack repair. The cracked samples were immersed in the NaCl solution for 4 weeks and then repaired using epoxy and cured for 14 days. The tensile stress and CMOD curves of the plain, pre-cracked, and crack-repaired (based on epoxy sealing) samples are shown in Fig. 12. Similar to the non-repaired 4-week corroded samples in Fig. 7, an increase in the tensile strength was not detected at the pre-crack width of 0.1 mm. When the pre-crack width was 0.3 mm or greater, the tensile strength of the UHPFRC increased owing to steel fiber corrosion for 4 weeks. When compared to the non-repaired corroded samples, a slightly higher increase in the tensile strength ratio (σ_{cr}/σ_{pc}) was observed in the repaired samples (i.e., C0.3- and C0.5–4R), as shown in Fig. 12b and c. This is because of the contribution of epoxy-based crack repair material to resist the pullout of steel fibers at the crack plane, although it showed a much lower bond strength than the UHPC matrix (Fig. 5). To quantitatively evaluate the increase of tensile strength ratio by the crack repair material, the tensile strength ratios were calculated and found to be 1.205 and 1.296 for the pre-crack width of 0.3 and 0.5 mm, respectively. Thus, increased tensile strengths of approximately 20–30% were attributed to the moderate steel fiber corrosion and crack repair material. The tensile strength increases by about 8–13%, which may be attributed to the crack repair material.

To evaluate the corrosion inhibition efficiency of the crack repair material, the 4-week corroded samples were repaired and then re-corroded in the NaCl solution for an additional 6 weeks. Thus, they were corroded intentionally for 10 weeks, equal to the non-repaired, 10-week corroded samples in Fig. 11. As shown in Fig. 13, there was no clear change in the tensile performance of C0.1–4R6 sample when compared to those of the control and pre-cracked samples. This is caused by the inhibition of NaCl solution

permeation by the repair material and dense interfacial zone between the fiber and matrix. The tensile strengths of the C0.3- and C0.5–4R6 samples were higher than those of the control and pre-cracked samples. Such an increase in the tensile strength was observed in the 4-week corroded samples with and without crack repairs. The tensile strength ratios (σ_{cr}/σ_{pc}) of the C0.3- and C0.5–4R6 samples were found to be approximately 1.23 and 1.35, respectively, which were slightly higher than those of the C0.3- and C0.5–4R samples. The increased tensile strengths were inconsistent with the results of the non-repaired C0.3- and C0.5-10 samples, showing reduced tensile strengths up to 11.4% (Fig. 11). This means that the epoxy-based repair material effectively prevents further permeation of the NaCl solution, delaying the corrosion progress of steel fibers located at the crack plane. This could be verified by microscope image and surface roughness in Figs. 8–10. The surface state of steel fiber from the C0.3–4R6 sample was slightly changed from the C0.3-4 sample, relative to that of C0.3-10 sample. As compared to the C0.3-10 sample, smaller amounts of ferric oxide formed at the exposed and boundary regions and much lower surface roughness were detected in the C0.3–4R6 sample, indicating the effective suppress of further corrosion. However, the values of R_a slightly increased by additional corrosion process for 6 weeks (C0.3-4 → C0.3–4R6) due to a formation of slight ferric oxides from remaining NaCl solution. Therefore, repairing cracks formed in the UHPFRC with a width of 0.3 mm or greater is important to inhibit corrosion progress of the steel fibers. Owing to very tiny microcrack formation and high content of unhydrated particles remained, it has been known that UHPFRC has self-healing capacity [55–57]. Based on previous studies [28,58], the crack self-healing in UHPFRC is effective to improve corrosion resistance of steel fibers through microcracks, but if cracks are partially self-healed due to various causes, e.g., wide crack width, insufficient ionic calcium (Ca^{2+}) contents, short healing duration, etc., the steel fibers are gradually corroded when exposed to corrosive environments. The epoxy-injected crack repairing method, however, could effectively fill up the cracks up to 0.5 mm and suppress the steel fibers from further corrosion.

4. Conclusions

This study evaluated the advantages of crack repair using epoxy sealing on the resistance of steel fiber corrosion for cracked UHPFRC. Three pre-crack widths of 0.1–0.5 mm and two corrosion durations of 4 and 10 weeks were adopted for cracked UHPFRC with and without repair. To evaluate the effect of epoxy-based repair material on the corrosion resistance of steel fibers, the degree of surface corrosion was quantitatively evaluated using a confocal laser scanning microscope. The conclusions can be drawn from the results obtained, as follows:

1) The average bond strength of smooth, straight steel fiber from UHPC was found to be 7.73 MPa. An identical steel fiber from the repair material provided the bond strength of 1.70 MPa, approximately 22% of that from the UHPC matrix.
2) The tensile performance of UHPFRC with the smallest crack width of 0.1 mm was marginally changed under corrosive environments for up to 10 weeks. A wider crack width accelerated the corrosion of the steel fibers and significantly affected the post-cracking tensile performance.
3) Considering the corrosion duration of 4 weeks, the tensile strengths of cracked UHPFRC with a width of 0.3 mm or greater increased by approximately 11.8–16.9%. However, the increased tensile strengths were mitigated at the longer corrosion duration of 10 weeks, and the 0.5-mm cracked UHPFRC showed even 11.4% lower tensile strength owing to fiber ruptures.
4) The crack repair material contributed to the increase in the tensile strength of the cracked UHPFRC after its exposure to the 4-week corrosive environment by approximately 10%. It effectively prevented further corrosion of steel fibers located at the crack surface, leading to higher tensile strengths even after the 10-week corrosion.

In this study, the effectiveness of epoxy injection repair process on inhibiting further steel fiber corrosion in UHPFRC was verified by a lab test. However, for its practical application, various curing environments for the epoxy repairing material need to be investigated, including an aggressive chloride-rich environmental condition.

Declaration of Competing Interest

There is no conflict of interest.

Acknowledgements

This work was supported by the National Research Foundation of Korea grant funded by the Korea government (MSIT) (No. 2021R1A2C4001503).

REFERENCES

[1] Batson G. Steel fiber reinforced concrete. Mater Sci Eng 1976;25:53–8.
[2] Bentur A, Mindess S. Fibre reinforced cementitious composites. CRC Press; 2006.
[3] Song PS, Hwang S, Sheu BC. Strength properties of nylon-and polypropylene-fiber-reinforced concretes. Cement Concr Res 2005;35(8):1546–50.
[4] Banthia N, Sappakittipakorn M. Toughness enhancement in steel fiber reinforced concrete through fiber hybridization. Cement Concr Res 2007;37(9):1366–72.
[5] Raza SS, Qureshi LA, Ali B, Raza A, Khan MM. Effect of different fibers (steel fibers, glass fibers, and carbon fibers) on mechanical properties of reactive powder concrete. Struct Concr 2021;22(1):334–46.
[6] Passuello A, Moriconi G, Shah SP. Cracking behavior of concrete with shrinkage reducing admixtures and PVA fibers. Cement Concr Compos 2009;31(10):699–704.
[7] Hsie M, Tu C, Song PS. Mechanical properties of polypropylene hybrid fiber-reinforced concrete. Mater Sci Eng 2008;494(1–2):153–7.

[8] Yoo DY, Moon DY. Effect of steel fibers on the flexural behavior of RC beams with very low reinforcement ratios. Construct Build Mater 2018;188:237–54.
[9] Chiaia B, Fantilli AP, Vallini P. Combining fiber-reinforced concrete with traditional reinforcement in tunnel linings. Eng Struct 2009;31(7):1600–6.
[10] Bayasi Z, McIntyre M. Application of fibrillated polypropylene fibers for restraint of plastic shrinkage cracking in silica fume concrete. ACI Mater J 2002;99(4):337–44.
[11] Banthia N, Gupta R. Influence of polypropylene fiber geometry on plastic shrinkage cracking in concrete. Cement Concr Res 2006;36(7):1263–7.
[12] Naaman AE, Reinhardt HW. Proposed classification of HPFRC composites based on their tensile response. Mater Struct 2006;39(5):547–55.
[13] Richard P, Cheyrezy M. Composition of reactive powder concretes. Cement Concr Res 1995;25(7):1501–11.
[14] Toutlemonde F, Resplendino J. Designing and building with UHPFRC: state of the art and development. London-New York: Wiley-ISTE; 2011. p. 814.
[15] Toutlemonde F, Resplendino J. AFGC-ACI-fib-RILEM international conference on ultra-high performance fibre-reinforced concrete building with UHPFRC: new large-scale implementations, recent technical advances, experience and standards. In: Proceedings of the international symposium on ultra-high performance fibre-reinforced concrete. RILEM publications S.A.R.L., proceedings PRO 106. 2 volumes; 2017. p. 1128.
[16] Graybeal B, Brühwiler E, Kim BS, Toutlemonde F, Voo YL, Zaghi A. International perspective on UHPC in bridge engineering. J Bridge Eng 2020;25(11):04020094.
[17] Yoo DY, Yoon YS. A review on structural behavior, design, and application of ultra-high-performance fiber-reinforced concrete. Int J Concr Struct Mater 2016;10(2):125–42.
[18] AFGC. Ultra high performance fibre-reinforced concretes. Interim Recommendations. Bagneux, France: AFGC publication; 2013.
[19] ACI Committee 239. Ultra-high performance concrete. Toronto, Ontario, Canada: ACI Fall Convention; 2012.
[20] Voort TLV. Design and field testing of tapered H-shaped ultra high performance concrete piles. MS Thesis. Iowa, USA: Iowa State University; 2008. p. 229.
[21] Hashimoto K, Toyoda T, Yokota H, Kono T, Kawaguchi T. Tension-softening behavior and chloride ion diffusivity of cracked ultra-high strength fiber reinforced concrete. In: RILEM-fib-AFGC international symposium on ultra high performance fibre-reinforced concrete, Marseille, France; 2013. p. 257–64.
[22] Beglarigale A, Yazıcı H. Electrochemical corrosion monitoring of steel fiber embedded in cement based composites. Cement Concr Compos 2017;83:427–46.
[23] Shaheen E, Shrive NG. Optimization of mechanical properties and durability of reactive powder concrete. ACI Mater J 2006;103(6):444–547.
[24] Kosa K, Naaman AE. Corrosion of steel fiber reinforced concrete. ACI Mater J 1990;87(1):27–37.
[25] Abbas S, Soliman AM, Nehdi ML. Chloride ion penetration in reinforced concrete and steel fiber-reinforced concrete precast tunnel lining segments. ACI Mater J 2014;111(6):613–22.
[26] Yoo DY, Min KH, Lee JH, Yoon YS. Shrinkage and cracking of restrained ultra-high-performance fiber-reinforced concrete slabs at early age. Construct Build Mater 2014;73:357–65.
[27] Berrocal CG, Löfgren I, Lundgren K, Tang L. Corrosion initiation in cracked fibre reinforced concrete: influence of crack width, fibre type and loading conditions. Corrosion Sci 2015;98:128–39.
[28] Shin W, Yoo DY. Influence of steel fibers corroded through multiple microcracks on the tensile behavior of ultra-high-performance concrete. Construct Build Mater 2020;259:120428.
[29] NF P18-710. National addition to eurocode 2 — design of concrete structures: specific rules for ultra-high performance fibre-reinforced concrete (UHPFRC). France: Francis de Pressensé; 2016.
[30] Pyo S, Koh T, Tafesse M, Kim HK. Chloride-induced corrosion of steel fiber near the surface of ultra-high performance concrete and its effect on flexural behavior with various thickness. Construct Build Mater 2019;224:206–13.
[31] Xi Y, Siemer DD, Scheetz BE. Strength development, hydration reaction and pore structure of autoclaved slag cement with added silica fume. Cement Concr Res 1997;27(1):75–82.
[32] Yoo DY, Kang ST, Yoon YS. Effect of fiber length and placement method on flexural behavior, tension-softening curve, and fiber distribution characteristics of UHPFRC. Construct Build Mater 2014;64:67–81.
[33] Yoo DY, Kim S, Kim JJ, Chun B. An experimental study on pullout and tensile behavior of ultra-high-performance concrete reinforced with various steel fibers. Construct Build Mater 2019;206:46–61.
[34] ASTM C39/39M. Standard test method for compressive strength of cylindrical concrete specimens. West Conshohocken, PA: ASTM International; 2014. p. 1–7.
[35] Lee NK, Koh KT, Park SH, Ryu GS. Microstructural investigation of calcium aluminate cement-based ultra-high performance concrete (UHPC) exposed to high temperatures. Cement Concr Res 2017;102:109–18.
[36] You I, Yoo DY, Kim S, Kim MJ, Zi G. Electrical and self-sensing properties of ultra-high-performance fiber-reinforced concrete with carbon nanotubes. Sensors 2017;17(11):2481.
[37] Farooq M, Banthia N. FRP fibre-cementitious matrix interfacial bond under time-dependent loading. Mater Struct 2019;52(6):1–11.
[38] Park JS, Kim YJ, Cho JR, Jeon SJ. Early-age strength of ultra-high performance concrete in various curing conditions. Materials 2015;8(8):5537–53.
[39] Xu M, Hallinan B, Wille K. Effect of loading rates on pullout behavior of high strength steel fibers embedded in ultra-high performance concrete. Cement Concr Compos 2016;70:98–109.
[40] Won JP, Hong BT, Lee SJ, Choi SJ. Bonding properties of amorphous micro-steel fibre-reinforced cementitious composites. Compos Struct 2013;102:101–9.
[41] JSCE. Recommendations for design and construction of high performance fiber reinforced cement composites with multiple fine cracks (HPFRCC). Japan: Japan Society of Civil Engineers; 2008.
[42] Kang ST, Kim JK. The relation between fiber orientation and tensile behavior in an ultra high performance fiber reinforced cementitious composites (UHPFRCC). Cement Concr Res 2011;41(10):1001–14.
[43] Van Belleghem B, Kessler S, Van den Heede P, Van Tittelboom K, De Belie N. Chloride induced reinforcement corrosion behavior in self-healing concrete with encapsulated polyurethane. Cement Concr Res 2018;113:130–9.
[44] Roventi G, Bellezze T, Giuliani G, Conti C. Corrosion resistance of galvanized steel reinforcements in carbonated concrete: effect of wet–dry cycles in tap water and in chloride solution on the passivating layer. Cement Concr Res 2014;65:76–84.
[45] https://usa.sika.com/content/dam/dms/us01/b/pds-cpd-Sikadur35HiModLVLPL-us.pdf.

[46] Jones S, Martys N, Lu Y, Bentz D. Simulation studies of methods to delay corrosion and increase service life for cracked concrete exposed to chlorides. Cement Concr Compos 2015;58:59–69.
[47] Wille K, Naaman AE. Effect of ultra-high-performance concrete on pullout behavior of high-strength brass-coated straight steel fibers. ACI Mater J 2013;110(4):451–61.
[48] Yoo DY, Gim JY, Chun B. Effects of rust layer and corrosion degree on the pullout behavior of steel fibers from ultra-high-performance concrete. J Mater Res Technol 2020;9(3):3632–48.
[49] Frazão C, Barros J, Camões A, Alves AC, Rocha L. Corrosion effects on pullout behavior of hooked steel fibers in self-compacting concrete. Cement Concr Res 2016;79:112–22.
[50] Ngo TT, Tran NT, Kim DJ, Pham TC. Effects of corrosion level and inhibitor on pullout behavior of deformed steel fiber embedded in high performance concrete. Construct Build Mater 2021;280:122449.
[51] Yoo DY, Shin W, Banthia N. Corrosion of partially and fully debonded steel fibers from ultra-high-performance concrete and its influence on pullout resistance. Cement Concr Compos 2021;124:104269.
[52] van Tol AF, Tibballs JE, Gjerdet NR, Ellison P. Experimental investigation of the effect of surface roughness on bone-cement-implant shear bond strength. J Mech Behav Biomed Mater 2013;28:254–62.
[53] Chun B, Yoo DY, Banthia N. Achieving slip-hardening behavior of sanded straight steel fibers in ultra-high-performance concrete. Cement Concr Compos 2020;113:103669.
[54] Frazão C, Díaz B, Barros J, Bogas JA, Toptan F. An experimental study on the corrosion susceptibility of recycled steel fiber reinforced concrete. Cement Concr Compos 2019;96:138–53.
[55] Beglarigale A, Eyice D, Tutkun B, Yazıcı H. Evaluation of enhanced autogenous self-healing ability of UHPC mixtures. Construct Build Mater 2021;280:122524.
[56] Doostkami H, Roig-Flores M, Serna P. Self-healing efficiency of ultra high-performance fiber-reinforced concrete through permeability to chlorides. Construct Build Mater 2021;310:125168.
[57] Kim S, Yoo DY, Kim MJ, Banthia N. Self-healing capability of ultra-high-performance fiber-reinforced concrete after exposure to cryogenic temperature. Cement Concr Compos 2019;104:103335.
[58] Yoo DY, Shin W, Chun B, Banthia N. Assessment of steel fiber corrosion in self-healed ultra-high-performance fiber-reinforced concrete and its effect on tensile performance. Cement Concr Res 2020;133:106091.